

# The final stages of accretion onto non-Kerr compact objects

Cosimo Bambi<sup>1,2,\*</sup> and Enrico Barausse<sup>3,†</sup>

<sup>1</sup>*Institute for the Physics and Mathematics of the Universe,  
The University of Tokyo, Kashiwa, Chiba 277-8583, Japan*

<sup>2</sup>*Arnold Sommerfeld Center for Theoretical Physics,  
Ludwig-Maximilians-Universität München, 80333 Munich, Germany*

<sup>3</sup>*Maryland Center for Fundamental Physics & Joint Space-Science Institute,  
Department of Physics, University of Maryland, College Park, MD 20742, USA*

(Dated: October 11, 2011)

The  $5 - 20M_{\odot}$  dark objects in X-ray binary systems and the  $10^5 - 10^9M_{\odot}$  dark objects in galactic nuclei are currently thought to be the Kerr black holes predicted by General Relativity. However, direct observational evidence for this identification is still elusive, and the only viable approach to confirm the Kerr black hole hypothesis is to explore and rule out any other possibility. Here we investigate the final stages of the accretion process onto generic compact objects. While for Kerr black holes and for more oblate bodies the accreting gas reaches the innermost stable circular orbit (ISCO) and plunges into the compact object, we find that for more prolate bodies several scenarios are possible, depending on the spacetime geometry. In particular, we find examples in which the gas reaches the ISCO, but then gets trapped between the ISCO and the compact object. In this situation, accretion onto the compact object is possible only if the gas loses additional angular momentum, forming torus-like structures inside the ISCO.

PACS numbers: 04.50.Kd, 97.10.Gz, 97.60.Lf

## I. INTRODUCTION

There is by now robust observational evidence supporting the existence of  $5 - 20M_{\odot}$  dark objects in X-ray binary systems and that of  $10^5 - 10^9M_{\odot}$  dark objects in galactic nuclei [1]. These objects are thought to be the black holes (BHs) predicted by General Relativity (GR), since their characteristics cannot be explained otherwise without introducing new physics. In 4-dimensional GR, an (uncharged) stationary BH is described by the Kerr solution and is uniquely characterized by two parameters, the mass  $M$  and the spin angular momentum  $J$  [2]. A fundamental limit for a Kerr BH is the bound  $|a| \leq 1$ , where  $a = cJ/(GM^2)$  is the spin parameter, which ensures that the Kerr metric describes a BH and not a naked singularity.

However, the evidence that the geometry around these BH candidates is described by the Kerr metric is still circumstantial, and the Kerr BH hypothesis mainly relies on the assumption that GR is the correct theory of gravity. Because GR has been tested only in the weak-field regime [3], several authors have suggested possible ways to further test the Kerr BH hypothesis using future, and in some cases even present, data.

More specifically, the detection of extreme mass ratio inspirals (EMRIs, i.e. systems consisting of a stellar-mass compact object orbiting a supermassive BH candidate) with future space-based gravitational-wave detectors will allow one to map the spacetime geometry with exquisite accuracy. This is because missions like LISA

or a similar European mission will be able to follow the stellar-mass compact object for millions of orbits around the central supermassive BH candidate, and therefore deviations from the Kerr geometry will lead to a phase difference in the gravitational waveforms that grows with the number of observed cycles. This technique is very promising and has been studied in detail by many authors [4–6]. Likewise, future gravitational-wave detectors will be able to detect the quasi-normal modes of BH candidates, and because for a Kerr BH the frequencies of these modes depend only on the spacetime’s mass  $M$  and spin  $J$ , any departure from this pattern will allow one to measure deviations away from the Kerr geometry [7].

The geometry around BH candidates can be constrained also with present or future electromagnetic data. For instance, radio timing observations allow constraints to be put on the quadrupole moment of the compact companions of radio pulsars [8], while astrometric monitoring of stars orbiting at milliparsec distances from Sgr A\* may be used to constrain models for the supermassive BH candidate at the center of the Galaxy [9]. Constraints on the nature of BH candidates can also be obtained by extending the methods currently used to estimate the spins of these objects, such as X-ray continuum [10] and iron-K $\alpha$  measurements [11], observations of quasi-periodic oscillations [12], and measurements of the cosmic X-ray background [13]. These methods can in principle be applied even with present data, provided that the systematic errors are properly understood. Future observations of the shadow of nearby supermassive BH candidates are another exciting possibility to test the BH paradigm [14].

BH candidates are often surrounded by an accretion disk. For the stellar-mass objects in X-ray binary systems, the disk originates from the material stripped from

\* cosimo.bambi@ipmu.jp

† barausse@umd.edu

the companion, while the gas accreting onto the super-massive objects in galactic nuclei comes from the interstellar medium. When the mass accretion rate is moderate and the accreting gas has significant angular momentum, the disk is geometrically thin and optically thick. The standard framework to describe these disks is the Novikov-Thorne model [15], where the disk lies on the equatorial plane of the system and the gas moves on nearly geodesic circular orbits. If the central object is a BH, the inner edge of the disk is assumed to be at the radius of the innermost stable circular orbit (ISCO): circular orbits inside the ISCO are radially unstable, so the gas reaches the ISCO moving on quasi-circular orbits, and then quickly plunges into the BH. A crucial ingredient of the Novikov-Thorne model is the assumption that the gas does not emit additional radiation as soon as it enters the plunging region. Numerical simulations show that deviations from this picture are small relative to the effect of the uncertainties in other parameters of the system [16] and can therefore be neglected. (Note however that the authors of Ref. [17] reach a different conclusion, because using general relativistic magnetohydrodynamics simulations they find that there can be significant magnetic stress inside the ISCO.)

If the central object is not a Kerr BH, the final stages of the accretion process may be different. In this work we focus on the so-called Manko-Novikov (MN) spacetimes [18]. These are stationary, axisymmetric, and asymptotically flat exact solutions of the vacuum Einstein equations with arbitrary mass-multipole moments, and they can therefore describe the geometry outside a generic compact object, be it a Kerr black hole or some other exotic object within GR. In particular, we consider a subclass of MN spacetimes characterized by three parameters (mass  $M$ , spin angular momentum  $J$  and mass quadrupole moment  $Q$ ). In a Kerr spacetime, the quadrupole moment  $Q_{\text{Kerr}}$  and all the higher order multipole moments are known to be functions of the mass and spin. Thus, if  $Q = Q_{\text{Kerr}}(M, J)$  our MN spacetimes exactly reduce to a Kerr BH. This property is very convenient because it makes these spacetimes an ideal tool to set-up a null experiment to test the BH paradigm: any experiment pointing at a value of  $Q$  significantly different from  $Q_{\text{Kerr}}(M, J)$  would imply that the object under consideration is either a compact object different from a BH within GR, or a BH or a compact object in a gravity theory different from GR. In this sense, MN spacetimes can be used not only to test the BH hypothesis but also to test the gravity theory itself.

The accretion process in our MN spacetimes can be qualitatively different than in a Kerr spacetime. In particular, we find that when the accreting gas reaches the ISCO (i.e. the inner edge of the Novikov-Thorne disk model) there are four qualitatively different possibilities:

1. The ISCO is *radially* unstable, and the gas plunges into the compact object remaining roughly on the equatorial plane. This is the same scenario as in the Kerr case.
2. The ISCO is *radially* unstable and the gas plunges, but does not reach the compact object. Instead, it gets trapped between the object and the ISCO and forms a thick disk.
3. The ISCO is *vertically* unstable, and the gas plunges into the compact object *outside* the equatorial plane.
4. The ISCO is *vertically* unstable and the gas plunges, but does not reach the compact object. Instead, it gets trapped between the object and the ISCO and forms two thick disks, above and below the equatorial plane.

This paper is organized as follows. In Sec. II we review a subclass of the MN solutions, characterized by three free parameters  $(M, J, Q)$ , that we use to describe the spacetime around generic compact objects. In Sec. III, we study plunging orbits in these MN spacetimes and we show that the accreting gas may not reach the surface of the compact object. This may lead to the formation of a thick disk inside the ISCO. In Sec. IV we discuss the possible astrophysical consequences of these thick disks. Finally, in Sec. V we draw our conclusions, while in Appendix A we review the theory of thick non-gravitating disks in axisymmetric stationary spacetimes, which we use to describe the thick disks inside the ISCO. In Appendix B we review the thermal bremsstrahlung emission rate.

Throughout the paper we use units in which  $G = c = 1$ , unless stated otherwise.

## II. MANKO-NOVIKOV SPACETIMES

The MN metric [18] is a stationary, axisymmetric, and asymptotically flat exact solution of the Einstein vacuum equations with arbitrary mass-multipole moments. In quasi-cylindrical coordinates  $(\rho, z)$  and in prolate spheroidal coordinates  $(x, y)$ , the line element is, respectively,

$$\begin{aligned}
 ds^2 &= -f (dt - \omega d\phi)^2 + \frac{e^{2\gamma}}{f} (d\rho^2 + dz^2) + \frac{\rho^2}{f} d\phi^2 = \\
 &= -f (dt - \omega d\phi)^2 + \frac{k^2 e^{2\gamma}}{f} (x^2 - y^2) \left( \frac{dx^2}{x^2 - 1} + \frac{dy^2}{1 - y^2} \right) + \frac{k^2}{f} (x^2 - 1) (1 - y^2) d\phi^2,
 \end{aligned} \tag{2.1}$$

where

$$f = e^{2\psi} A/B, \quad \omega = 2ke^{-2\psi} CA^{-1} - 4k\alpha(1 - \alpha^2)^{-1}, \quad e^{2\gamma} = e^{2\gamma'} A(x^2 - 1)^{-1}(1 - \alpha^2)^{-2}, \quad (2.2)$$

and

$$\psi = \sum_{n=1}^{+\infty} \frac{\alpha_n P_n}{R^{n+1}}, \quad (2.3)$$

$$\begin{aligned} \gamma' = \frac{1}{2} \ln \frac{x^2 - 1}{x^2 - y^2} + \sum_{m,n=1}^{+\infty} \frac{(m+1)(n+1)\alpha_m \alpha_n}{(m+n+2)R^{m+n+2}} (P_{m+1}P_{n+1} - P_m P_n) + \\ + \left[ \sum_{n=1}^{+\infty} \alpha_n \left( (-1)^{n+1} - 1 + \sum_{k=0}^n \frac{x-y+(-1)^{n-k}(x+y)}{R^{k+1}} P_k \right) \right], \end{aligned} \quad (2.4)$$

$$A = (x^2 - 1)(1 + \tilde{a}\tilde{b})^2 - (1 - y^2)(\tilde{b} - \tilde{a})^2, \quad (2.5)$$

$$B = [x + 1 + (x - 1)\tilde{a}\tilde{b}]^2 + [(1 + y)\tilde{a} + (1 - y)\tilde{b}]^2, \quad (2.6)$$

$$C = (x^2 - 1)(1 + \tilde{a}\tilde{b})[\tilde{b} - \tilde{a} - y(\tilde{a} + \tilde{b})] + (1 - y^2)(\tilde{b} - \tilde{a})[1 + \tilde{a}\tilde{b} + x(1 - \tilde{a}\tilde{b})], \quad (2.7)$$

$$\tilde{a} = -\alpha \exp \left[ \sum_{n=1}^{+\infty} 2\alpha_n \left( 1 - \sum_{k=0}^n \frac{(x-y)}{R^{k+1}} P_k \right) \right], \quad (2.8)$$

$$\tilde{b} = \alpha \exp \left[ \sum_{n=1}^{+\infty} 2\alpha_n \left( (-1)^n + \sum_{k=0}^n \frac{(-1)^{n-k+1}(x+y)}{R^{k+1}} P_k \right) \right]. \quad (2.9)$$

Here  $R = \sqrt{x^2 + y^2 - 1}$  and  $P_n$  are the Legendre polynomials with argument  $xy/R$ ,

$$\begin{aligned} P_n = P_n \left( \frac{xy}{R} \right), \\ P_n(\chi) = \frac{1}{2^n n!} \frac{d^n}{d\chi^n} (\chi^2 - 1)^n, \end{aligned} \quad (2.10)$$

while the relation between prolate spheroidal and quasi-cylindrical coordinates is given by

$$\rho = k\sqrt{(x^2 - 1)(1 - y^2)}, \quad z = kxy, \quad (2.11)$$

with inverse

$$\begin{aligned} x = \frac{1}{2k} \left( \sqrt{\rho^2 + (z+k)^2} + \sqrt{\rho^2 + (z-k)^2} \right), \\ y = \frac{1}{2k} \left( \sqrt{\rho^2 + (z+k)^2} - \sqrt{\rho^2 + (z-k)^2} \right). \end{aligned} \quad (2.12)$$

The MN solution has an infinite number of free parameters:  $k$ , which regulates the mass of the spacetime;  $\alpha$ , which regulates the spin; and  $\alpha_n$  ( $n = 1, \dots, +\infty$ ) which regulates the mass-multipole moments, starting from the dipole  $\alpha_1$ , to the quadrupole  $\alpha_2$ , etc. For  $\alpha \neq 0$  and  $\alpha_n = 0$ , the MN solution reduces to the Kerr metric. For  $\alpha = \alpha_n = 0$ , it reduces to the Schwarzschild solution. For  $\alpha = 0$  and  $\alpha_n \neq 0$ , one obtains the static Weyl metric.

The no-hair theorem [19] states that the only asymptotically flat, vacuum and stationary solution of the Einstein equations that is non-singular on and outside an event horizon and that presents no closed timelike curves outside it is given by the Kerr metric. Therefore, the MN

spacetime must either have no event horizon, or present naked singularities or closed timelike curves outside it. In fact, the surface  $x = 1$  ( $\rho = 0$ ,  $|z| \leq k$ ), which is the event horizon in the Kerr case  $\alpha_n = 0$ , in general is only a partial horizon, because it presents a naked curvature singularity on the equatorial plane (i.e. at  $x = 1$ ,  $y = 0$ , corresponding to  $\rho = z = 0$ ) [18]. Also, there are closed timelike curves outside it. However, these pathological features appear at small radii and here the basic idea is that naked singularities and closed timelike curves do not exist in reality because they are either inside some sort of exotic compact object, whose *exterior* gravitational field is described by the MN metric, or because GR breaks down close to them; see e.g. Ref. [20] for some specific mechanisms that can do the job.

Without loss of generality, we can put  $\alpha_1 = 0$  to bring the massive object to the origin of the coordinate system. In what follows, we restrict our attention to the subclass of MN spacetimes with  $\alpha_n = 0$  for  $n \neq 2$ . We then have three free parameters ( $k$ ,  $\alpha$ , and  $\alpha_2$ ) related to the mass  $M$ , the dimensionless spin parameter  $a = J/M^2$ , and the dimensionless anomalous quadrupole moment  $q = -(Q - Q_{\text{Kerr}})/M^3$ , by the relations

$$\alpha = \frac{\sqrt{1 - a^2} - 1}{a}, \quad (2.13)$$

$$k = M \frac{1 - \alpha^2}{1 + \alpha^2}, \quad (2.14)$$

$$\alpha_2 = q \frac{M^3}{k^3}. \quad (2.15)$$

Note that  $q$  measures the deviation from the quadrupole moment of a Kerr BH. In particular, since  $Q_{\text{Kerr}} = -a^2 M^3$ , the solution is oblate for  $q > -a^2$  and prolate for  $q < -a^2$ . When  $q = 0$ , the solution reduces to the Kerr metric, but when  $q \neq 0$  also the higher-order mass-multipole moments have a different value than in Kerr.

Because the MN metric is stationary and axisymmetric, geodesic orbits have two constants of motion, the specific energy  $E = -u_t$  and the  $z$ -component of the specific angular momentum  $L = u_\phi$ . The  $t$ - and  $\phi$ -components of the 4-velocity of a test-particle are therefore

$$u^t = \frac{E g_{\phi\phi} + L g_{t\phi}}{g_{t\phi}^2 - g_{tt} g_{\phi\phi}}, \quad (2.16)$$

$$u^\phi = -\frac{E g_{t\phi} + L g_{tt}}{g_{t\phi}^2 - g_{tt} g_{\phi\phi}}. \quad (2.17)$$

From the normalization of the 4-velocity,  $g_{\mu\nu} u^\mu u^\nu = -1$ , we can write

$$\frac{e^{2\gamma}}{f} [(u^\rho)^2 + (u^z)^2] = V_{\text{eff}}(E, L, \rho, z), \quad (2.18)$$

where the effective potential  $V_{\text{eff}}$  is defined by

$$V_{\text{eff}} = \frac{E^2}{f} - \frac{f}{\rho^2} (L - \omega E)^2 - 1. \quad (2.19)$$

Circular orbits in the equatorial plane must have  $\dot{\rho} = \dot{z} = 0$ , which implies  $V_{\text{eff}} = 0$ , and  $\ddot{\rho} = \ddot{z} = 0$ , which implies  $\partial_\rho V_{\text{eff}} = 0$  and  $\partial_z V_{\text{eff}} = 0$ . This means that circular equatorial orbits are located at simultaneous zeros and extrema of the effective potential, where  $\partial_\rho V_{\text{eff}} = \partial_z V_{\text{eff}} = V_{\text{eff}} = 0$ . Because  $\partial_z V_{\text{eff}} = 0$  is satisfied identically for  $z = 0$  (simply because of the reflection symmetry of the MN metric with respect to the equatorial plane), from these conditions one can obtain  $E$  and  $L$  as a function of the radius  $r$  of the circular equatorial orbit. These orbits are stable under small perturbations in the radial direction if  $\partial_\rho^2 V_{\text{eff}} < 0$ , and in the vertical direction if  $\partial_z^2 V_{\text{eff}} < 0$ .

As far as the position of the ISCO is concerned, for any given value of  $a$  there are two critical values  $q_1$  and  $q_2$  for the anomalous quadrupole moment (both negative,  $q_2 < q_1 < 0$ , but whose exact values depend on the spin  $a$ ). For  $q \geq q_1$ , circular orbits on the equatorial plane are always vertically stable and the ISCO radius is determined by the onset of the orbital instability in the radial direction (i.e. the ISCO is the marginally stable circular orbit in the radial direction). This is the picture that one is familiar with in the Kerr case, which is indeed included in this range of  $q$ 's (since for Kerr  $q = 0$ ).

For  $q_2 < q < q_1$ , there are two circular orbits  $r = r_1$  and  $r = r_2$  (with  $r_1 > r_2$ ) that are vertically stable but only marginally stable in the radial direction, and one circular orbit  $r = r_3$  (with  $r_3 < r_2$ ) that is radially stable but only marginally stable in the vertical direction. Stable circular orbits therefore exist for  $r > r_1$  and for  $r_3 < r < r_2$ , while orbits with  $r_2 < r < r_1$  are radially unstable (although vertically stable) and orbits with  $r <$

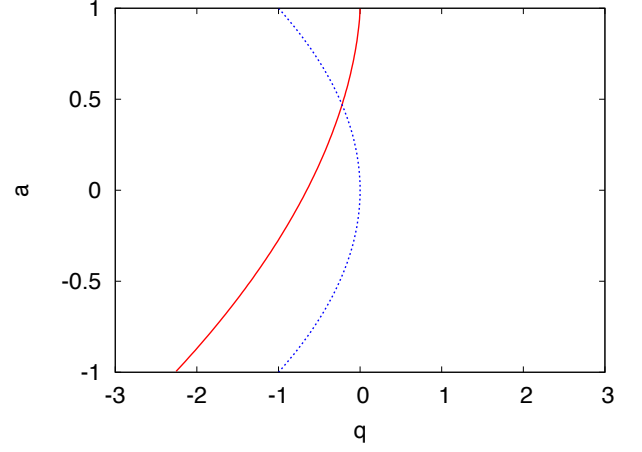


FIG. 1. The character of the effective ISCO for MN spacetimes with spin parameter  $a$  and anomalous quadrupole moment  $q$ . Compact objects to the right (left) of the solid red line have ISCOs determined by the instability in the radial (vertical) direction. Compact objects to the right (left) of the dotted blue line are oblate (prolate) bodies, while they are more oblate (prolate) than a BH if  $q > 0$  ( $q < 0$ ).

$r_3$  are vertically unstable (although radially stable). As far as an accretion disk is concerned, however, what is relevant is the radius  $r = r_1$  of the outer marginally stable circular orbit, because that is the radius at which the gas starts plunging. We thus dub the circular orbit at  $r = r_1$  the “effective” ISCO. It is important to notice, however, that the stable orbits in the “inner” region  $r_3 < r < r_2$  do *not* necessarily have energy and angular momentum larger than those of the effective ISCO. For this reason, plunging orbits starting at the effective ISCO may hit a potential barrier preventing them from reaching the compact object, at least in some regions of the parameter space  $(a, q)$ . We will study this situation in detail in the next section.

As  $q$  decreases towards  $q_2$ , the values of  $r_1$  and  $r_2$  approach and eventually coincide for  $q = q_2$ . For  $q < q_2$ , there are no marginally stable orbits in the radial direction, i.e. all circular orbits are radially stable. However, the marginally stable orbit in the vertical direction,  $r = r_3$ , still exists and marks the position of the ISCO, which is therefore determined by the onset of the vertical instability.

In conclusion, for  $q > q_2(a)$  [with  $q_2(a) < 0$ ], the effective ISCO for quasi-circular inspirals is given by the onset of the radial instability, while for  $q < q_2(a)$  it is determined by the onset of the vertical instability. Also, let us note that the critical value  $q_2$  may be larger than  $-a^2$ , that is, the ISCO can be determined by the vertical instability even for oblate objects (although since  $q_2 < 0$  these objects need to be less oblate than a Kerr BH). This situation is summarized in Fig. 1, where we show the regions in the  $(a, q)$  plane where compact objects are prolate/oblate and more prolate/more oblate than a Kerr BH, and the regions where the effective ISCO is deter-

mined by the vertical/radial instability.

In the rest of this paper we will present our results for MN spacetimes in terms of the standard Boyer-Lindquist coordinates  $(r, \theta)$ , which are related to the prolate spheroidal coordinates  $(x, y)$  and the quasi-cylindrical coordinates  $(\rho, z)$  used in this section by

$$\begin{aligned}\rho &= \sqrt{r^2 - 2Mr + a^2 M^2} \sin \theta, \\ z &= (r - M) \cos \theta.\end{aligned}\quad (2.20)$$

and

$$\begin{aligned}r &= kx + M, \\ \cos \theta &= y.\end{aligned}\quad (2.21)$$

Also, hereafter we will use coordinates in which the mass  $M$  of the MN metric is 1.

### III. THE PLUNGE AND THE FORMATION OF THICK DISKS INSIDE THE ISCO

At the inner edge of the thin accretion disk, which corresponds to the effective ISCO defined in the previous section, the gas is expected to shed and plunge towards the central object. To understand the geometry of this plunge, it is convenient to plot the region accessible to the shedding gas, i.e. the region accessible to particles having the ISCO specific energy and angular momentum  $E_{\text{ISCO}}$  and  $L_{\text{ISCO}}$ . This “plunge” region is defined by

$$V_{\text{eff}}(E_{\text{ISCO}}, L_{\text{ISCO}}, r, \theta) \geq 0, \quad (3.1)$$

and automatically includes the ISCO ( $r = r_{\text{ISCO}}$ ,  $\theta = \pi/2$ ), but not necessarily a neighborhood of it. More specifically, one can have several scenarios:

1. If the effective ISCO is determined by the onset of the radial instability, there are two possibilities:
  - (a) The gas plunges directly into the compact object. As in the Kerr case, the “plunge” region and therefore the gas may expand above and below the equatorial plane forming a sort of “plume”, but they remain confined near the equatorial plane.
  - (b) The gas starts to plunge from the ISCO, but gets trapped before reaching the compact object.
2. If the effective ISCO is determined by the onset of the vertical instability, there are three possibilities:
  - (a) The gas plunges directly into the compact object. However, because the ISCO is stable in the radial direction, the gas does not shed on the equatorial plane as in the Kerr case, but sheds above and below the equatorial plane, forming two separate “plumes”.

- (b) The “plunge” region does not contain a neighborhood of the ISCO, because  $V_{\text{eff}}(E_{\text{ISCO}}, L_{\text{ISCO}}, r, \theta)$  is strictly negative around it. However, a small perturbation (e.g. a small initial velocity) is enough to allow the gas to escape the potential well surrounding the ISCO, thus shedding above and below the equatorial plane and plunging into the compact object in two separate plumes. Note that this case is therefore very similar to scenario (2a).
- (c) The gas sheds above and below the equatorial plane from the ISCO, but gets trapped before reaching the compact object.

Scenarios (1b) and (2c), where the gas sheds from the inner edge of the thin disk but gets trapped before reaching the compact object, are clearly non-stationary configurations, because the gas keeps accumulating between the object and the ISCO. For the system to settle onto a stationary configuration, the gas would have to overflow the potential barrier separating it from the object, but this can be achieved only if the gas forms, inside the ISCO, a coherent structure that is capable of further dissipating energy and angular momentum (e.g. through viscosity or magnetic fields).

In this paper we study these “coherent structures” inside the ISCO using the theory of non self-gravitating, stationary and axisymmetric thick disks developed in Refs. [21, 22] (see also Refs. [5, 23, 24]). We will briefly review this formalism in Appendix A, but for the present discussion it is sufficient to mention that a thick disk is completely determined by specifying its inner or outer edge and the angular momentum distribution on the equatorial plane. More precisely, one needs to assume a certain equatorial distribution for the angular momentum per unit energy  $\ell = L/E$ , and this distribution completely determines the distribution  $\ell(r, \theta)$  of the angular momentum per unit energy outside the equatorial plane (see Appendix A for details). Assuming in particular a power law, we can write

$$\bar{\ell}(r) \equiv \ell(r, \theta = \pi/2) = \ell_{\text{ISCO}} \left( \frac{r}{r_{\text{ISCO}}} \right)^\beta, \quad (3.2)$$

where  $\ell_{\text{ISCO}} = L_{\text{ISCO}}/E_{\text{ISCO}}$  and  $\beta$  is a free parameter, which needs to be positive in order for the thick disk to be stable [23].

In our case, we impose that the outer edge of the thick disk coincides with the ISCO (so that the thick disk is fed by the gas shedding from the thin disk), and we choose the parameter  $\beta$  such that the thick disk also presents an inner shedding point. This requirement completely fixes the value of  $\beta$  to a certain critical value  $\beta_{\text{crit}}$ . The gas shedding from the inner edge of the thick disk will then plunge into the compact object, and the “plunge” region accessible to this gas will be described by

$$V_{\text{eff}}(E_{\text{inner}}, L_{\text{inner}}, r, \theta) \geq 0, \quad (3.3)$$

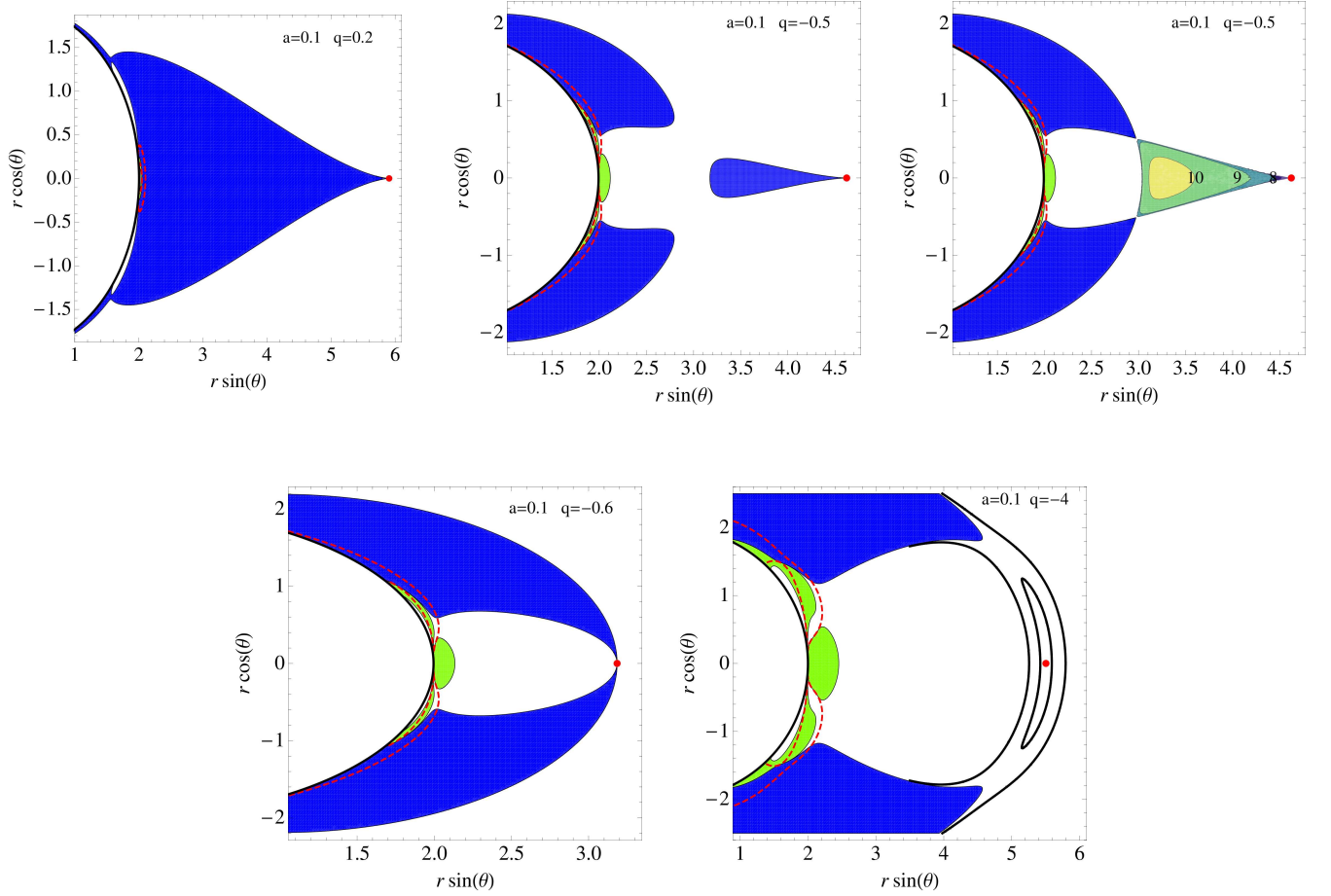


FIG. 2. Accretion in Manko-Novikov spacetimes with  $a = 0.1$  and  $q = 0.2, -0.5, -0.6$  and  $q = -4$ . The solid black line at small radii is the partial horizon  $x = 1$ , the region where closed timelike curves exist (i.e. the region where  $g_{\phi\phi} < 0$ ) is shown in green/light gray, the red dashed line is the boundary of the ergoregion (i.e.  $g_{tt} = 0$  on that line), while the red dot on the equatorial plane marks the position of the ISCO, i.e. the inner edge of the thin accretion disk. The thick disk, if it forms, sheds from the ISCO and is denoted by concentric contours, whose label is an upper limit to the  $\log_{10}$  of the gas temperature in K (see text for details). In blue/dark grey is the region accessible to the gas shedding from the inner edges of the thick disk [i.e. the region where  $V_{\text{eff}}(E_{\text{inner}}, L_{\text{inner}}, r, \theta) \geq 0$ ,  $E_{\text{inner}}$  and  $L_{\text{inner}}$  being the energy and angular momentum of the gas at the inner edges of the thick disk]. If no thick disk is present, in blue/dark grey is the region accessible to the gas shedding from the inner edge of the thin disk [i.e. the region where  $V_{\text{eff}}(E_{\text{ISCO}}, L_{\text{ISCO}}, r, \theta) \geq 0$ ]: if this “plunge” region does not reach the ISCO, we also show (with solid black lines around the ISCO) the contours  $V_{\text{eff}}(E_{\text{ISCO}}, L_{\text{ISCO}}, r, \theta) = -10^{-4}$  and  $V_{\text{eff}}(E_{\text{ISCO}}, L_{\text{ISCO}}, r, \theta) = -10^{-3}$ , which represent the region where the gas reaching the ISCO can shed if subject to a small perturbation.

For  $q = 0.2$  the ISCO is radially unstable, and the gas plunges directly into the compact object remaining roughly on the equatorial plane, as in the Kerr case [scenario (1a)]. For  $q = -0.5$  the ISCO is radially unstable and the gas plunges, but does not reach the compact object; instead, it gets trapped between the object and the ISCO and forms a thick disk [scenario (1b)]. For  $q = -0.6$  the ISCO is vertically unstable, and the gas plunges directly into the compact object outside the equatorial plane [scenario (2a)]. For  $q = -4$  the ISCO is vertically unstable, and the gas does not plunge directly but remains trapped in the vicinities of the ISCO [because  $V_{\text{eff}}(E_{\text{ISCO}}, L_{\text{ISCO}}, r, \theta) < 0$  near the ISCO]. However, the potential barrier is not tall enough to allow a thick disk to form, and a small perturbation is enough to cause the gas to fall into the central object [scenario (2b)].

where the specific energy and angular momentum of the gas at the inner edge of the thick disk,  $E_{\text{inner}}$  and  $L_{\text{inner}}$ , are determined by solving simultaneously  $L_{\text{inner}}/E_{\text{inner}} = \ell(r_{\text{inner}}, \theta_{\text{inner}})$  and  $V_{\text{eff}}(E_{\text{inner}}, L_{\text{inner}}, r_{\text{inner}}, \theta_{\text{inner}}) = 0$ .

Examples of the scenario outlined above are shown in Figs. 2 (for  $a = 0.1$ ), 3 (for  $a = 0.5$ ) and 4 (for  $a = 0.9$ ), for various values of the anomalous quadrupole moment

$q$ . The solid black line at small radii is the partial horizon  $x = 1$ , the region where closed timelike curves exist (i.e. the region where  $g_{\phi\phi} < 0$ ) is shown in green/light gray, while the red dashed line is the boundary of the ergoregion (i.e.  $g_{tt} = 0$  on that line). The position of the ISCO is marked by a red dot on the equatorial plane. The thick disk, if it forms, sheds from the ISCO



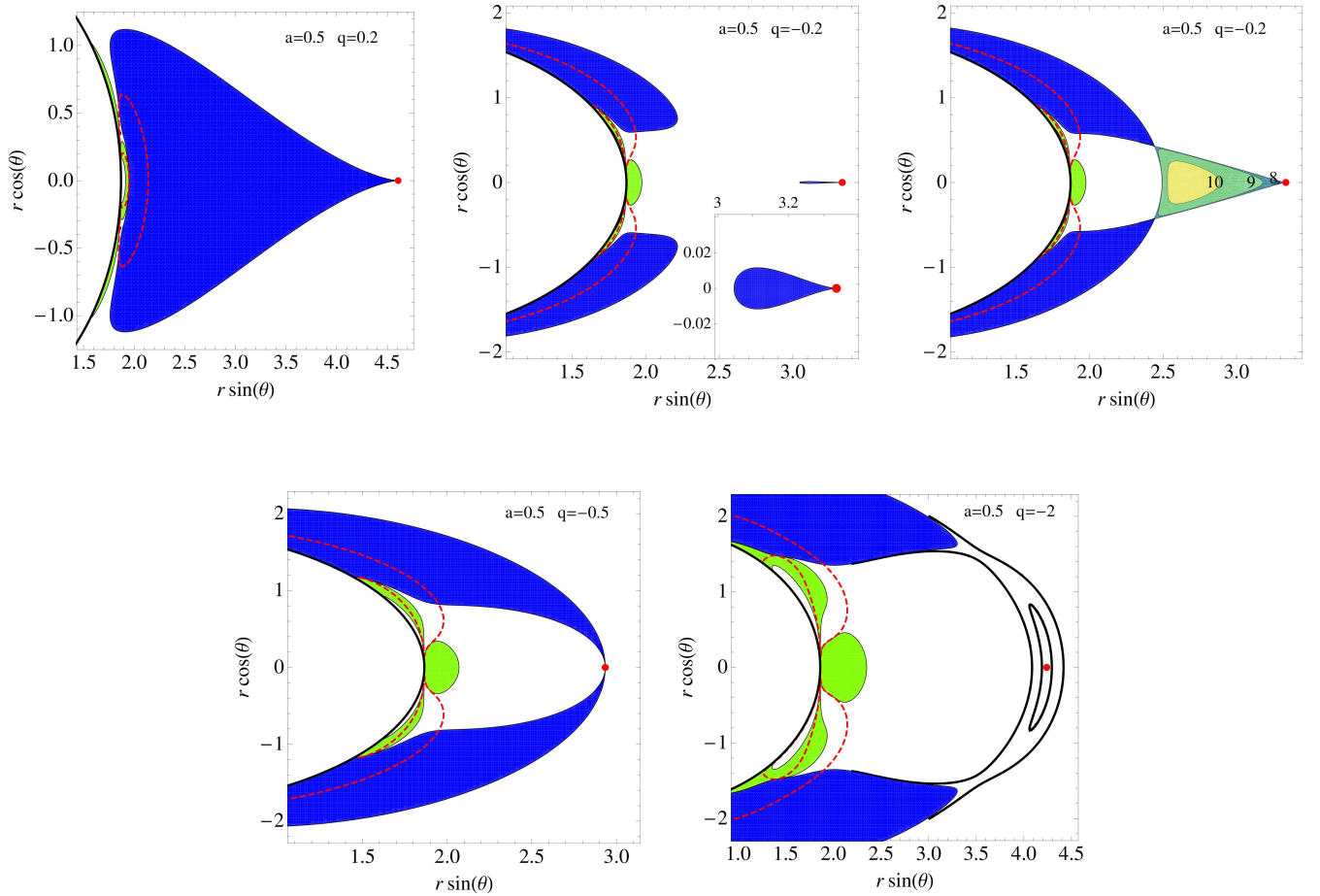


FIG. 3. Same notation as in Fig. 2, but for  $a = 0.5$  and  $q = 0.2, -0.2, -0.5$  and  $-2$ . The accretion properties too are qualitatively similar, case by case, to those displayed for  $a = 0.1$  in Fig. 2.

and is denoted by concentric contours, whose label is  $\log_{10} T$ , where  $T$  is the gas temperature (in K) assuming a polytropic equation of state  $p = \kappa \rho_0^\Gamma$  ( $\rho_0$  being the rest mass density) with  $\Gamma = 2$ . As we will show in Appendix A, the temperature for other values of the polytropic index  $\Gamma$  can be obtained by the simple rescaling  $T(\Gamma) = T(\Gamma = 2) \times 2(\Gamma - 1)/\Gamma$ . Because the factor  $2(\Gamma - 1)/\Gamma$  varies between 0 and 1 when  $\Gamma$  varies in its allowed range  $1 < \Gamma < 2$ , the temperature plotted in our figures has to be interpreted as an upper value to the real temperature. In blue/dark grey is the “plunge” region accessible to the gas shedding from the inner edges of the thick disk [i.e. the region where  $V_{\text{eff}}(E_{\text{inner}}, L_{\text{inner}}, r, \theta) \geq 0$ ]. If no thick disk is present, in blue/dark grey is the “plunge” region accessible to the gas shedding from the inner edge of the thin disk [i.e. the region where  $V_{\text{eff}}(E_{\text{ISCO}}, L_{\text{ISCO}}, r, \theta) \geq 0$ ]: if this “plunge” region does not contain a neighborhood of the ISCO [cf. scenario (2b) above], we also show (with solid black lines around the ISCO) the contours  $V_{\text{eff}}(E_{\text{ISCO}}, L_{\text{ISCO}}, r, \theta) = -10^{-4}$  and  $V_{\text{eff}}(E_{\text{ISCO}}, L_{\text{ISCO}}, r, \theta) = -10^{-3}$ , which represent the region where the gas reaching the ISCO can move if subject to a small perturbation (e.g. if imparted a small

initial velocity).

As can be seen, scenarios (1a), (1b) and (2a) happen for all the three values of the spin parameter that we consider. In particular, although a more detailed scan of the parameter plane  $(a, q)$  would be needed to draw ultimate conclusions, it seems that scenario (1a) generically takes place when  $q > q_1(a)$ , scenario (1b) when  $q_2(a) < q < q_1(a)$ , and scenario (2a) when  $q < q_2(a)$ . However, for  $q < q_2(a)$  one can also have scenario (2b) – which we see for  $a = 0.1, q = -4$  and  $a = 0.5, q = -2$  – or scenario (2c) – which we see for  $a = 0.9$  and  $q = -0.12$ . We have not been able to identify a scenario (2c) for  $a = 0.1$  or  $a = 0.5$ . This is because for these values of the spin, the potential barrier preventing the gas shedding at the ISCO from plunging above and below the equatorial plane is smaller than for  $a = 0.9$ , and a small perturbation is sufficient for the gas to plunge, thus making the formation of a stationary thick disk impossible or at least very difficult. Mathematically, this means that when varying the exponent  $\beta$  in Eq. (3.2), we were unable to find a value  $\beta_{\text{crit}}$  for which the thick disk has an inner shedding point (and therefore a stationary configuration). Scenario (2c) is instead possible

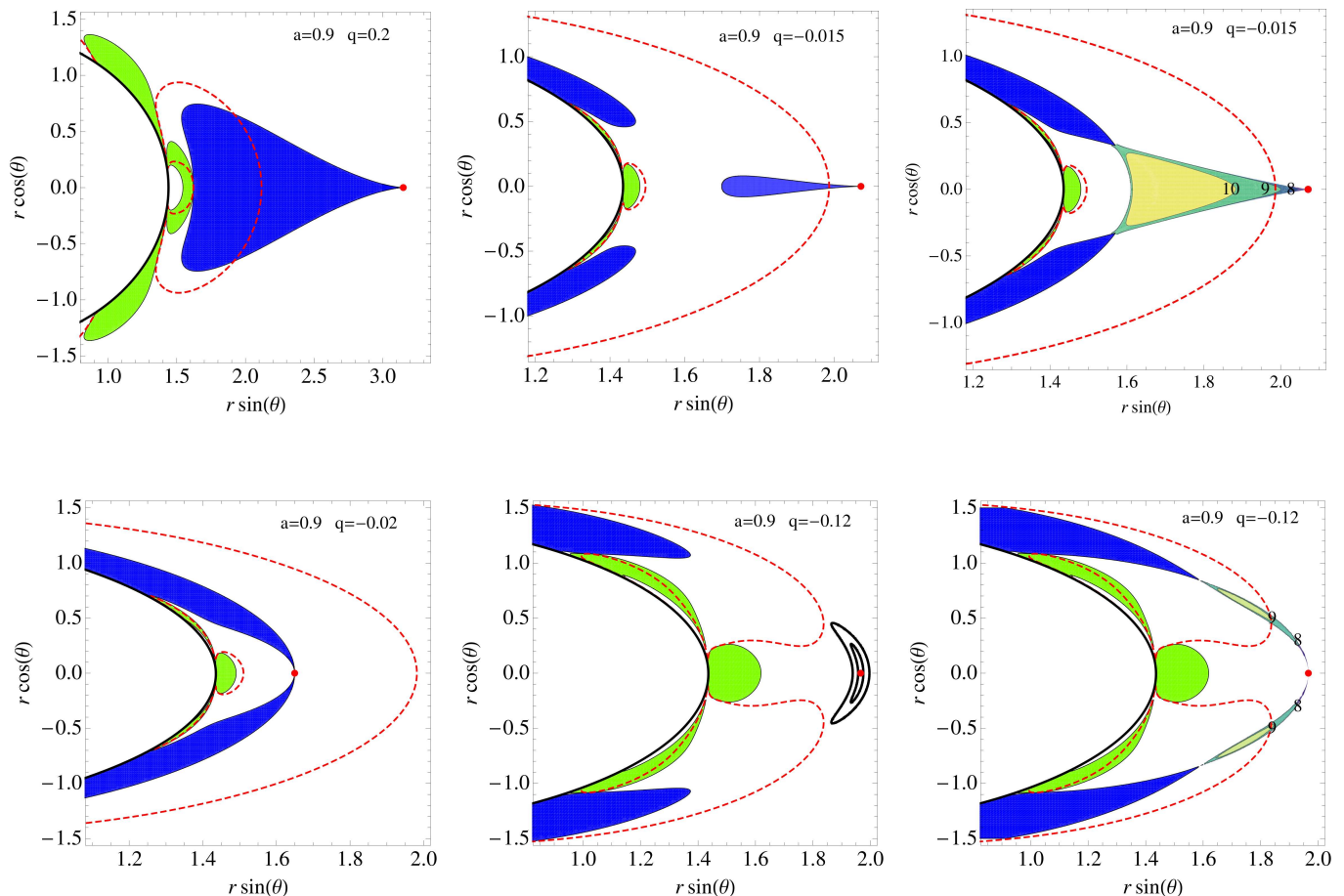


FIG. 4. Same notation as in Fig. 2, but for  $a = 0.9$  and  $q = 0.2, -0.015, -0.02$  and  $-0.12$ . The accretion properties are qualitatively similar to those displayed for  $a = 0.1$  in Fig. 2 and for  $a = 0.5$  in Fig. 3, except for  $q = -0.12$ . In that case, the ISCO is vertically unstable, and the gas does not plunge directly but remains trapped in the vicinities of the ISCO (because  $V_{\text{eff}}(E_{\text{ISCO}}, L_{\text{ISCO}}, r, \theta) < 0$  near the ISCO). However, the potential barrier is tall enough to allow the formation of two thick disks, above and below the equatorial plane [scenario (2c)]. This contrasts with the cases  $a = 0.1, q = -4$  (Fig. 2) and  $a = 0.2, q = -2$  (Fig. 3), where the potential barrier is smaller and can be easily overcome if the gas is slightly perturbed.

for  $a = 0.9$  because in that case the potential barrier is higher [cf. the contours  $V_{\text{eff}}(E_{\text{ISCO}}, L_{\text{ISCO}}, r, \theta) = -10^{-4}$  and  $V_{\text{eff}}(E_{\text{ISCO}}, L_{\text{ISCO}}, r, \theta) = -10^{-3}$  for  $a = 0.9$  and  $q = -0.12$  with those for  $a = 0.1, q = -4$  or  $a = 0.5, q = -2$ ].

Finally, let us comment on where the “surface” of the compact object may be located. As already mentioned, the MN metric is an exact vacuum solution of the Einstein equations, and describes the spacetime *outside* a generic compact object made of exotic matter, which determines the free parameters of the MN metric (e.g. the anomalous quadrupole moment  $q$ ). This object should of course cover the pathological features of the MN solutions, such as the closed timelike curves, the curvature singularity at  $x = 1, y = 0$  and the partial horizon  $x = 1, |y| \leq 1$ . Even if this were the case, however, this scenario would still present some difficulties. First, such an exotic compact object would probably be subject to gravitational instabilities on a dynamical timescale, unless its radius is large enough to cover the whole ergoregion. In

fact, the so-called ergoregion instability is known to happen on a dynamical timescale for objects whose exterior metric resembles that of Kerr BH, at least for spin parameters  $a \lesssim 2$  [25]. Second, if the compact object has a surface, the kinetic energy of the plunging material must eventually be emitted by the surface, while in the case of a BH it simply gets lost in the event horizon. This argument, coupled with the observation that BH candidates are indeed dimmer than systems known to contain neutron stars, or at least stars with a surface, is a strong indication of the existence of event horizons [26]. However, we should stress that one can in principle imagine models escaping this argument (e.g. a gravastar, where the radiation emitted by the surface is so redshifted that it becomes observationally negligible [27]).

Another possibility is that GR breaks down near the naked curvature singularity and the closed timelike curves of the MN geometry. One can therefore imagine a completely regular spacetime that is described by the MN metric away from the singularity and the closed



timelike curves, and which does not present these pathological features any more (see Refs. [20] for some explicit ideas in this direction). An advantage of this scenario is that the horizon of this “regular” MN spacetime would allow these objects to have a dimmer luminosity, in agreement with the observations [26], and it may even quench the ergoregion instability or make it happen on a non-dynamical timescale.

Of course, the MN spacetimes that we consider, irrespective of their actual physical significance, are also an ideal tool to set-up null experiments to test the Kerr BH hypothesis, since they reduce exactly to Kerr BHs when  $q = 0$ . Indeed, any experiment pointing at a value of  $q$  significantly different from 0 would imply that the object under consideration is either a compact object different from a BH within GR, or a BH or a compact object in a gravity theory different from GR. In this sense, MN spacetimes can be used not only to test the BH hypothesis but also to test the gravity theory itself [28].

#### IV. DISCUSSION

The scenario (1a) discussed in the previous section is, as we have mentioned, very similar to the accretion process in a Kerr spacetime. At the ISCO, which is radially unstable, the gas plunges into the compact object, remaining roughly on the equatorial plane. Because this plunge takes place in a dynamical time and with no significant dissipation, the infalling gas is not expected to emit a significant amount of radiation, and this is a crucial ingredient of the Novikov-Thorne model. Under this assumption, the accretion luminosity is simply  $L_{\text{acc}} = \eta \dot{M} c^2$ , where  $\eta = 1 - E_{\text{ISCO}}$  is the radiative efficiency. The evolution of the spin parameter is then regulated by [29]

$$\frac{da}{d \ln M} = \frac{1}{M} \frac{L_{\text{ISCO}}}{E_{\text{ISCO}}} - 2a, \quad (4.1)$$

neglecting the small correction coming from the radiation emitted by the disk and captured by the compact object.

In the case of a Kerr background, the Novikov-Thorne model seems to be confirmed by recent three-dimensional general relativistic magnetohydrodynamic simulations [16] (see however Ref. [17] for a different conclusion), and can therefore be used to interpret the X-ray spectra of BH candidates and estimate their spin [30]. It seems therefore plausible that the Novikov-Thorne model should work also in MN spacetimes, and in principle one can generalize the technique used to estimate the spin parameter of BH candidates to measure possible deviations from the Kerr geometry (e.g. the anomalous quadrupole moment  $q$ ) [10]. From Eq. (4.1), it also follows that the accretion process onto a compact object more oblate than a Kerr BH can potentially spin the body up to  $a > 1$  [31].

Scenarios (2a) and (2b) are quite similar to scenario (1a). In these cases the ISCO is vertically unstable, so the gas plunges above and below the equatorial plane,

but this infall still happens on a dynamical time and with a negligible emission of radiation. This presumably means that the Novikov-Thorne model is a reasonable description of the thin disk and that the spin of the central object evolves according to (4.1). Also, because the shape of the plunge region draws the gas towards the rotation axis, outflows and jets might possibly form in these scenarios if magnetic fields are present.

In scenarios (1b) and (2c), the assumption of no radiation emitted inside the ISCO is not valid, because of the presence of the thick disks that we discussed in the previous section. As a result, the radiative efficiency is not  $\eta = 1 - E_{\text{ISCO}}$  like in the Novikov-Thorne model, but  $\eta = 1 - E_{\text{inner}}$ , while the spin evolution of the central object is still described by Eq. (4.1), but with the ratio  $L_{\text{ISCO}}/E_{\text{ISCO}}$  replaced by  $L_{\text{inner}}/E_{\text{inner}}$ . The values of these quantities are shown in Table I for the cases shown in Figs. 2, 3 and 4, and as can be seen the corrections due to the presence of the thick disks inside the ISCO are about 1 – 3% for the ratio  $L_{\text{inner}}/E_{\text{inner}}$ , and about 10 – 25% when it comes to  $\eta$ .

Moreover, the spectrum of the thick disks inside the ISCO is quite different from that of the thin disk. The temperature of a thin disk scales like  $T \sim M^{-0.25}$ ,  $M$  being the disk’s mass, while the temperature of the thick disks inside the ISCO is independent of  $M$  (see Appendix A for details), like in the case of Bondi accretion flows. As can be seen from Figs. 2, 3 and 4, we have  $T \sim 10^9 - 10^{10}$  K  $\approx 0.1 - 1$  MeV in the thick disks, and at such high temperatures the most efficient cooling mechanism is thermal bremsstrahlung, whose emission rate is briefly reviewed in Appendix B.

In the case of a  $10 M_{\odot}$  compact object, for reasonable values of the gas density of the thick disks, e.g.  $10^{12}$  particles/cm<sup>3</sup>, the disk is definitely optically thin. The radiation emitted by the thick disk thus scales as  $M^3$ , but the flux observable on the Earth is completely negligible: considering an object at a distance of 1 kpc, the intensity of the  $\gamma$ -ray spectrum around 0.1 – 1 MeV is lower than  $10^{-15}$   $\gamma$  cm<sup>-2</sup> s<sup>-1</sup>. For a  $10^9 M_{\odot}$  compact object, the thick disk inside the ISCO is not necessarily optically thin, but if it is, the  $\gamma$ -ray spectrum of the object may include a bump around 0.1 – 1 MeV, with the characteristic shape of thermal bremsstrahlung (spectrum almost constant till energies  $\sim T$  and then exponentially suppressed). If the object is at 10 Mpc from us, the flux on the Earth could be around 1  $\gamma$  cm<sup>-2</sup> s<sup>-1</sup>, which is potentially observable. For instance, the so-called MeV-blazars show this feature [32]. Unfortunately, so far the spectrum of active galactic nuclei (AGN) is too poorly understood to say anything conclusive, but the presence of a thick disk inside the ISCO of the supermassive objects in galactic nuclei will likely be testable in the future.

Finally, let us comment that although the presence of thick disks inside the ISCO may be used, at least in principle, as an observational signature of the existence of non-Kerr compact objects, the scenarios (1b) and (2c) where these disks form seem to arise only in limited re-

| $a$ | $q$    | $\beta_{\text{crit}}$ | $1 - E_{\text{ISCO}}$ | $1 - E_{\text{inner}}$ | $L_{\text{ISCO}}/E_{\text{ISCO}}$ | $L_{\text{inner}}/E_{\text{inner}}$ |
|-----|--------|-----------------------|-----------------------|------------------------|-----------------------------------|-------------------------------------|
| 0.1 | -0.5   | 0.0187                | 0.069                 | 0.075                  | 3.454                             | 3.426                               |
| 0.5 | -0.2   | 0.074                 | 0.093                 | 0.117                  | 3.057                             | 2.990                               |
| 0.9 | -0.015 | 0.048                 | 0.167                 | 0.195                  | 2.448                             | 2.418                               |
| 0.9 | -0.12  | 0.204                 | 0.310                 | 0.332                  | 1.970                             | 1.921                               |

TABLE I. The effect of the thick disk on the accretion efficiency and on the spin evolution of the central object, for the cases considered in Figs. 2, 3 and 4 that present a thick disk inside the ISCO.

gions of the  $(a, q)$  plane. For instance, as we have mentioned in the previous section, scenario (1b) seems to be possible only in a narrow region at the transition between scenarios (1a) and (2a), while scenario (2c) seems only to be possible for sufficiently high spins.

## V. CONCLUSIONS

The  $5 - 20M_{\odot}$  compact objects in X-ray binary systems and the supermassive bodies in galactic nuclei are currently thought to be the Kerr BHs predicted by GR. The study of the electromagnetic radiation emitted in the accretion process onto these objects can be used to investigate their actual nature and therefore test the Kerr BH paradigm [10, 11, 13]. In this paper we have studied the final stages of accretion, when the gas reaches the inner edge of the thin accretion disk, located at the ISCO, and plunges into the compact object. We find that for non-Kerr compact objects this process is much more complicated than in the case of Kerr BH. More specifically, depending on the spin  $a$  and anomalous quadrupole moment  $q$  of the compact object we find essentially four possible scenarios:

1. The ISCO is *radially* unstable, and the gas plunges into the compact object remaining roughly on the equatorial plane and without emitting significant radiation. This is the same scenario as in the Kerr case.
2. The ISCO is *radially* unstable and the gas plunges, but does not reach the compact object. Instead, it gets trapped between the object and the ISCO, forming a thick disk with  $T \lesssim 10^{10}$  K and emitting by thermal bremsstrahlung.
3. The ISCO is *vertically* unstable, and the gas plunges into the compact object *outside* the equatorial plane and without emitting significant radiation.
4. The ISCO is *vertically* unstable and the gas plunges, but does not reach the compact object. Instead, it gets trapped between the object and the ISCO and forms two thick disks, above and below the equatorial plane. These thick disks have  $T \lesssim 10^{10}$  K and emit by thermal bremsstrahlung.

While the second and the fourth of these scenarios seem to happen only for objects more prolate than Kerr, and even in that case only in a limited region of the parameter space  $(a, q)$ , they are nevertheless possible and may be testable with future data. Our results therefore show that care is needed when using the Novikov-Thorne model with objects that are different from Kerr BHs, as the assumption of negligible radiation emission inside the ISCO may not be correct. In particular, an excess of emission due to the presence of a thick disk in the region inside the ISCO might bias measurements of the spin of BH candidates towards high values. It may be interesting to test this possibility with the spectra of high-spin BH candidates such as GRS 1915+105 [33], when future more accurate measurements of the distance to this object will be available. For the time being, however, despite the peculiar features of the accretion process that we discovered in this paper, compact objects more prolate than Kerr BHs cannot be ruled out by astrophysical observations.

## ACKNOWLEDGMENTS

We would like to thank Luciano Rezzolla for critically reading this manuscript and providing useful feedback. We are also grateful to Sergei Blinnikov for useful discussions and suggestions. The work of C.B. was supported by World Premier International Research Center Initiative (WPI Initiative), MEXT, Japan, and by the JSPS Grant-in-Aid for Young Scientists (B) No. 22740147. E.B. acknowledges support from NSF Grants PHY-0903631.

### Appendix A: The theory of non self-gravitating, stationary and axisymmetric fluid configurations

Here we briefly review the theory of non self-gravitating, stationary and axisymmetric fluid configurations in generic stationary and axisymmetric background spacetimes. For more details, we refer the reader to Refs. [21, 22] (but see also Refs. [5, 23, 24]).

We start by considering a perfect fluid with 4-velocity

$\mathbf{u}^{\text{fluid}}$ , which is described by the stress-energy tensor

$$\begin{aligned} T^{\mu\nu} &= (\rho + p)u_{\text{fluid}}^\mu u_{\text{fluid}}^\nu + pg^{\mu\nu} \\ &= \rho_0 h u_{\text{fluid}}^\mu u_{\text{fluid}}^\nu + pg^{\mu\nu}. \end{aligned} \quad (\text{A1})$$

Here  $p$ ,  $\rho_0$ ,  $\rho$  and  $h \equiv (p + \rho)/\rho_0$  are the pressure, rest-mass density, energy density and specific enthalpy. We also assume that the fluid is described by a polytropic equation of state  $p = \kappa \rho_0^\Gamma = \rho_0 \varepsilon (\Gamma - 1)$ , where  $\varepsilon = \rho/\rho_0 - 1$  is the internal energy per unit rest-mass, and  $\kappa$  and  $\Gamma$  are respectively the polytropic constant and polytropic index. Because we are neglecting the self-gravity of the fluid,  $\mathbf{g}$  is the background metric (i.e., in our case, the MN metric). We assume that the fluid moves on non-geodesic circular orbits with 4-velocity

$$\begin{aligned} \mathbf{u}^{\text{fluid}} &= A(r, \theta) \left[ \frac{\partial}{\partial t} + \Omega(r, \theta) \frac{\partial}{\partial \phi} \right] \\ &= U(r, \theta) [-dt + \ell(r, \theta) d\phi], \end{aligned} \quad (\text{A2})$$

where  $\Omega \equiv u_{\text{fluid}}^\phi / u_{\text{fluid}}^t$  is the angular velocity,  $A \equiv u_{\text{fluid}}^t$  is called the redshift factor,  $U \equiv -u_{\text{fluid}}^t$  is the energy per unit mass as measured at infinity and  $\ell \equiv -u_{\text{fluid}}^\phi / u_{\text{fluid}}^t$  is the angular momentum per unit energy as measured at infinity. Note that  $\ell$  is conserved for a stationary and axisymmetric flow in a stationary and axisymmetric space-time [34]. The angular momentum per unit energy and the angular velocity are related by

$$\Omega = -\frac{g_{t\phi} + g_{tt}\ell}{g_{\phi\phi} + g_{t\phi}\ell}, \quad \ell = -\frac{g_{t\phi} + g_{\phi\phi}\Omega}{g_{tt} + g_{t\phi}\Omega}, \quad (\text{A3})$$

while  $\mathbf{u}^{\text{fluid}} \cdot \mathbf{u}^{\text{fluid}} = -1$  implies

$$U = \sqrt{\frac{g_{t\phi}^2 - g_{tt}g_{\phi\phi}}{g_{tt}\ell^2 + 2g_{t\phi}\ell + g_{\phi\phi}}}, \quad (\text{A4})$$

$$A = \sqrt{\frac{-1}{g_{tt} + 2g_{t\phi}\Omega + g_{\phi\phi}\Omega^2}}, \quad (\text{A5})$$

$$AU = \frac{1}{1 - \Omega\ell}. \quad (\text{A6})$$

To calculate the structure of the fluid configuration, we use Euler's equation

$$a_{\text{fluid}}^\mu = -\frac{(g^{\mu\nu} + u_{\text{fluid}}^\mu u_{\text{fluid}}^\nu) \partial_\nu p}{p + \rho}, \quad (\text{A7})$$

where  $a_{\text{fluid}}^\mu$  is the fluid's 4-acceleration. If the pressure is assumed to depend only on  $r$  and  $\theta$  (which follows from the stationarity and axisymmetry of the fluid and geometry) and if the equation of state is barotropic [i.e., if  $\rho = \rho(p)$ ]<sup>1</sup>, one can express Eq. (A7) in terms of the gradient of a scalar potential  $W(p)$ :

$$a_{\text{fluid}}^\mu = \partial_\mu W, \quad W(p) = -\int^p \frac{dp'}{p' + \rho(p')}. \quad (\text{A8})$$

Also, from the definition of 4-acceleration and using Eqs. (A2), (A5), (A6) and the Killing equations  $\nabla_{(\mu} \xi_{\nu)} = 0$  for  $\xi = \partial/\partial t$  and  $\xi = \partial/\partial \phi$ , one obtains

$$a_{\text{fluid}}^\mu = \partial_\mu W = -\frac{\partial_\mu p}{p + \rho} = \partial_\mu \ln U - \frac{\Omega}{1 - \Omega\ell} \partial_\mu \ell. \quad (\text{A9})$$

Taking the derivative of this equation, antisymmetrizing and using the trivial fact that  $\partial_{[\mu\nu]} W = \partial_{[\mu\nu]} \ell = \partial_{[\mu\nu]} U = 0$ , we obtain  $\partial_{[\mu} \Omega \partial_{\nu]} \ell = 0$ . This implies  $\nabla \Omega \propto \nabla \ell$ , and therefore  $\ell$  and  $\Omega$  have the same contour levels [35]. One can then express  $\Omega$  as a function of  $\ell$ ,  $\Omega = \Omega(\ell)$ , and write Eq. (A9) in the integral form

$$\begin{aligned} W - W_{\text{out}} &= -\int_0^p \frac{dp'}{p' + \rho(p')} \\ &= \ln U - \ln U_{\text{out}} - \int_{\ell_{\text{out}}}^\ell \frac{\Omega(\ell') d\ell'}{1 - \Omega(\ell') \ell'}, \end{aligned} \quad (\text{A10})$$

where  $W_{\text{out}}$  and  $\ell_{\text{out}}$  are the potential and angular momentum per unit energy at the outer edge of the fluid configuration. (Of course,  $W_{\text{out}}$  and  $\ell_{\text{out}}$  can be replaced by the values of  $W$  and  $\ell$  at any other point of the fluid's boundary, e.g. the inner edge of the configuration if that is present.)

In practice, in order to calculate  $W - W_{\text{out}}$ , one specifies the functional form of  $\ell$  on the equatorial plane,  $\bar{\ell}(r) \equiv \ell(r, \theta = \pi/2)$ . From that, one can use Eq. (A3) to obtain the angular velocity on the equatorial plane,  $\bar{\Omega}(r) \equiv \Omega(r, \theta = \pi/2)$ , and calculate the integral in Eq. (A10) as

$$\int \frac{\Omega(\ell') d\ell'}{1 - \Omega(\ell') \ell'} = \int \frac{\bar{\Omega}(r')}{1 - \bar{\Omega}(r') \bar{\ell}(r')} \frac{d\bar{\ell}(r')}{dr'} dr'. \quad (\text{A11})$$

To calculate  $\ln U(r, \theta)$ , one needs instead to reconstruct the functional form of  $\ell(r, \theta)$  outside the equatorial plane. This can be done by solving  $\Omega(r, \theta) = \bar{\Omega}(\bar{r})$  for the equatorial radius  $\bar{r}$  where the angular velocity has the same value as at a given point  $(r, \theta)$  outside the equatorial plane. Using Eq. (A3) and the fact that  $\Omega(r, \theta) = \bar{\Omega}(\bar{r})$  implies  $\ell(r, \theta) = \bar{\ell}(\bar{r})$  (because  $\ell$  and  $\Omega$  have the same contour levels), this equation becomes

$$\frac{g_{t\phi}(r, \theta) + g_{tt}(r, \theta) \bar{\ell}(\bar{r})}{g_{\phi\phi}(r, \theta) + g_{t\phi}(r, \theta) \bar{\ell}(\bar{r})} = \frac{\bar{g}_{t\phi}(\bar{r}) + \bar{g}_{tt}(\bar{r}) \bar{\ell}(\bar{r})}{\bar{g}_{\phi\phi}(\bar{r}) + \bar{g}_{t\phi}(\bar{r}) \bar{\ell}(\bar{r})}, \quad (\text{A12})$$

where we have denoted with  $\bar{g}_{\mu\nu}$  the metric on the equatorial plane. This equation is known as the equation of the von Zeipel cylinders, and by allowing one to express  $\bar{r}$  as a function of  $r$  and  $\theta$ , it permits calculating both  $\Omega(r, \theta)$  and  $\ell(r, \theta)$  outside the equatorial plane.

The integral Euler equation (A10) can be further simplified if the equation of state is polytropic, because in this case

$$\int_0^p \frac{dp'}{p' + \rho(p')} = \ln \frac{h}{h_{\text{out}}}, \quad (\text{A13})$$

<sup>1</sup> This is the case for a polytropic equation of state, as  $\rho = p/(\Gamma - 1) + (p/\kappa)^{1/\Gamma}$ .

where  $h_{\text{out}}$  is the specific enthalpy at the outer edge of the fluid configuration. Because for a polytropic equation of state the enthalpy is

$$h = 1 + \frac{\Gamma}{\Gamma - 1} \kappa \rho_0^{\Gamma-1}, \quad (\text{A14})$$

one has  $h_{\text{out}} = 1$  (because  $p = \rho_0 = 0$  at the outer edge of the fluid configuration), and Eqs. (A10) and (A13) give

$$\rho_0(r, \theta) = \left\{ \frac{\Gamma - 1}{\Gamma} \frac{[e^{W_{\text{out}} - W(r, \theta)} - 1]}{\kappa} \right\}^{1/(\Gamma-1)}, \quad (\text{A15})$$

which makes it clear that the fluid occupies the region where  $W(r, \theta) \leq W_{\text{out}}$ .

Once the rest-mass distribution is known, the total rest mass is

$$M_{t,0} = \int \rho_0 \sqrt{-g} u_{\text{fluid}}^t d^3x, \quad (\text{A16})$$

where  $d^3x = dr d\theta d\phi$  is the coordinate 3-volume element, while the mass-energy is

$$M_t = \int (T_r^r + T_\phi^\phi + T_\theta^\theta - T_t^t) \sqrt{-g} d^3x. \quad (\text{A17})$$

From Eq. (A15) one can also calculate the temperature using  $p = nk_B T$  (where  $k_B$  is the Boltzmann constant and  $n$  is the number density). Using the polytropic equation of state, one gets

$$T = \frac{m_p \kappa \rho_0^{\Gamma-1}}{k_B} = \frac{2(\Gamma - 1)}{\Gamma} \times \frac{m_p [e^{W_{\text{out}} - W(r, \theta)} - 1]}{2k_B}, \quad (\text{A18})$$

where we have assumed that the mass of the gas particles is given by the proton mass  $m_p$ . We notice that the

temperature is independent of the mass of the fluid configuration, and that the factor  $2(\Gamma - 1)/\Gamma$  varies between 0 and 1 when  $\Gamma$  varies in its allowed range  $1 < \Gamma < 2$ .

## Appendix B: Thermal bremsstrahlung

The emission rate per unit volume for a fully ionized hydrogen gas due to bremsstrahlung processes is [36]

$$\Lambda_{\text{brems}} = \alpha r_e^2 m_e c^3 n^2 F(\Theta_e), \quad (\text{B1})$$

where  $\alpha = 1/137$  is the electromagnetic fine structure constant,  $r_e$  is the classical electron radius,  $m_e$  is the electron mass,  $c$  is the speed of light,  $n$  is the number density of electrons (protons), and  $\Theta_e = k_B T_e / m_e c^2$  is the dimensionless electron temperature. Here  $F$  is the dimensionless radiation rate due to relativistic bremsstrahlung. It is convenient to write  $F = F_{ee} + F_{ep}$ , where  $F_{ee}$  is the contribution from electron-electron collisions, while  $F_{ep}$  the one from electron-proton collisions. For  $\Theta_e \leq 1$ , the approximated formulas are

$$\begin{aligned} F_{ee} &= \frac{20}{9\sqrt{\pi}} (44 - 3\pi^2) \Theta_e^{1.5} (1 + 1.1\Theta_e + \Theta_e^2 - 1.25\Theta_e^{2.5}) \\ F_{ep} &= \frac{32}{3} \sqrt{\frac{2}{\pi}} \Theta_e^{0.5} (1 + 1.78\Theta_e^{1.34}). \end{aligned} \quad (\text{B2})$$

For  $\Theta_e \geq 1$ , we have instead

$$\begin{aligned} F_{ee} &= 24\Theta_e [\ln(2\eta_E \Theta_e) + 1.25], \\ F_{ep} &= 12\Theta_e [\ln(2\eta_E \Theta_e + 0.42) + 1.5], \end{aligned} \quad (\text{B3})$$

where  $\eta_E = \exp(-\gamma_E)$  and  $\gamma_E \approx 0.5772$  is the Euler's number.

- 
- [1] R. Narayan, New J. Phys. **7**, 199 (2005).
  - [2] B. Carter, Phys. Rev. Lett. **26**, 331 (1971); D. C. Robinson, Phys. Rev. Lett. **34**, 905 (1975); P. T. Chrusciel and J. Lopes Costa, arXiv:0806.0016 (2008).
  - [3] C. M. Will, Living Rev. Rel. **9**, 3 (2005).
  - [4] F. D. Ryan, Phys. Rev. D **52**, 5707 (1995); **56**, 1845 (1997); **56**, 7732 (1997); N. A. Collins and S. A. Hughes, Phys. Rev. D **69**, 124022 (2004); K. Glampedakis and S. Babak, Class. Quant. Grav. **23**, 4167 (2006); L. Barack and C. Cutler, Phys. Rev. D **75**, 042003 (2007); T. A. Apostolatos, G. Lukes-Gerakopoulos and G. Contopoulos, Phys. Rev. Lett. **103**, 111101 (2009); G. Lukes-Gerakopoulos, T. A. Apostolatos and G. Contopoulos, Phys. Rev. D **81**, 124005 (2010); M. Kesden, J. Gair and M. Kamionkowski, Phys. Rev. D **71**, 044015 (2005); E. Barausse, L. Rezzolla, D. Petroff and M. Ansorg, Phys. Rev. D **75**, 064026 (2007); S. J. Vigeland and S. A. Hughes, Phys. Rev. D **81**, 024030 (2010); S. Vigeland, N. Yunes and L. Stein, Phys. Rev. D **83**, 104027 (2011); B. Kocsis, N. Yunes and A. Loeb, arXiv:1104.2322 (2011); N. Yunes, B. Kocsis, A. Loeb and Z. Haiman, arXiv:1103.4609 (2011); C. F. Sopuerta and N. Yunes, Phys. Rev. D **80**, 064006 (2009); P. Pani, V. Cardoso, L. Gualtieri, Phys. Rev. D **83**, 104048 (2011); E. Barausse and T. P. Sotiriou, Phys. Rev. Lett. **101**, 099001 (2008); J. R. Gair, E. E. Flanagan, S. Drasco, T. Hinderer and S. Babak, Phys. Rev. D **83**, 044037 (2011).
  - [5] E. Barausse and L. Rezzolla, Phys. Rev. D **77**, 104027 (2008).
  - [6] J. R. Gair, C. Li, I. Mandel, Phys. Rev. D **77**, 024035 (2008).
  - [7] E. Berti, V. Cardoso, Int. J. Mod. Phys. D **15**, 2209 (2006); E. Berti, V. Cardoso and A. O. Starinets, Class. Quant. Grav. **26**, 163001 (2009); C. B. M. Chirenti and L. Rezzolla, Class. Quant. Grav. **24**, 4191 (2007).
  - [8] N. Wex and S. M. Kopeikin, Astrophys. J. **514**, 388 (1999)

- [9] C. M. Will, *Astrophys. J. Lett.* **674**, L25 (2008); D. Merritt, T. Alexander, S. Mikkola and C. M. Will, *Phys. Rev. D* **81**, 062002 (2010)
- [10] C. Bambi, E. Barausse, *Astrophys. J.* **731**, 121 (2011); T. Harko, Z. Kovács and F. S. N. Lobo, *Class. Quant. Grav.* **26**, 215006 (2009); **27**, 105010 (2010); *Class. Quant. Grav.* **28**, 165001 (2011); *Phys. Rev. D* **79**, 064001 (2009).
- [11] T. Johannsen and D. Psaltis, arXiv:1011.4078 (2010)
- [12] T. Johannsen and D. Psaltis, *Astrophys. J.* **726**, 11 (2011).
- [13] C. Bambi, *Phys. Rev. D* **83**, 103003 (2011).
- [14] C. Bambi, K. Freese, *Phys. Rev. D* **79**, 043002 (2009); C. Bambi, K. Freese and R. Takahashi, arXiv:0908.3238 (2009); C. Bambi and N. Yoshida, *Class. Quant. Grav.* **27**, 205006 (2010); L. Amarilla, E. F. Eiroa and G. Gribet, *Phys. Rev. D* **81**, 124045 (2010); T. Johannsen, D. Psaltis, *Astrophys. J.* **716**, 187 (2010); **718**, 446 (2010).
- [15] I. D. Novikov, K. S. Thorne, “Astrophysics of Black Holes” in *Black Holes*, edited by C. De Witt and B. De Witt (Gordon and Breach, New York, New York, 1973), pp. 343-450; D. N. Page, K. S. Thorne, *Astrophys. J.* **191**, 499-506 (1974).
- [16] R. F. Penna, J. C. McKinney, R. Narayan, A. Tchekhovskoy, R. Shafee, J. E. McClintock, *Mon. Not. Roy. Astron. Soc.* **408**, 752 (2010); A. K. Kulkarni, R. F. Penna, R. V. Shcherbakov, J. F. Steiner, R. Narayan, A. Sadowski, Y. Zhu, J. E. McClintock, S. W. Davis and J. C. McKinney, *Mon. Not. Roy. Astron. Soc.* **414**, 1183 (2011).
- [17] S. C. Noble, J. H. Krolik, J. D. Schnittman, J. F. Hawley, arXiv:1105.2825 (2011).
- [18] V. S. Manko and I. D. Novikov, *Class. Quant. Grav.* **9**, 2477 (1992).
- [19] W. Israel, *Phys. Rev.* **164**, 1776 (1967); *Commun. Math. Phys.* **8**, 245 (1968); B. Carter, *Phys. Rev. Lett.* **26**, 331 (1971); S. W. Hawking, *Commun. Math. Phys.* **25**, 152 (1972); D. C. Robinson, *Phys. Rev. Lett.* **34**, 905 (1975).
- [20] E. K. Boyda, S. Ganguli, P. Horava and U. Varadarajan, *Phys. Rev. D* **67**, 106003 (2003); D. Israel, *JHEP* **0401**, 042 (2004); N. Drukker, *Phys. Rev. D* **70**, 084031 (2004).
- [21] M. Kozłowski, M. Jaroszynski, M. A. Abramowicz, *Astron. Astrophys.* **63**, 209 (1978).
- [22] M. A. Abramowicz, M. Jaroszynski, M. Sikora, *Astron. Astrophys.* **63**, 221 (1978).
- [23] J. A. Font and F. Daigne, *Mon. Not. Roy. Astron. Soc.* **334**, 383 (2002); F. Daigne and J. A. Font, *Mon. Not. Roy. Astron. Soc.* **349**, 841 (2004).
- [24] O. Zanotti, L. Rezzolla and J. A. Font, *Mon. Not. Roy. Astron. Soc.* **341**, 832 (2003); O. Zanotti, J. A. Font, L. Rezzolla and P. Montero, *Mon. Not. Roy. Astron. Soc.* **356**, 1371 (2005); P. J. Montero, O. Zanotti, J. A. Font, L. Rezzolla, *Mon. Not. Roy. Astron. Soc.* **378**, 1101-1110 (2007).
- [25] V. Cardoso, P. Pani, M. Cadoni, M. Cavaglia, *Phys. Rev. D* **77**, 124044 (2008); P. Pani, E. Barausse, E. Berti, V. Cardoso, *Phys. Rev.* **D82**, 044009 (2010).
- [26] A. E. Broderick and R. Narayan, *Astrophys. J. Lett.* **638**, L21 (2006); A. E. Broderick, A. Loeb and R. Narayan *Astrophys. J. Lett.* **701**, 1357 (2009).
- [27] M. A. Abramowicz, W. Kluzniak and J. P. Lasota, *Astron. Astrophys.* **396**, L31 (2002).
- [28] S. A. Hughes, arXiv:gr-qc/0608140 (2006).
- [29] J. M. Bardeen, *Nature* **226**, 64 (1970).
- [30] L. -X. Li, E. R. Zimmerman, R. Narayan, J. E. McClintock, *Astrophys. J. Suppl.* **157**, 335-370 (2005); J. E. McClintock, R. Narayan, S. W. Davis, L. Gou, A. Kulkarni, J. A. Orosz, R. F. Penna, R. A. Remillard *et al.*, *Class. Quant. Grav.* **28**, 114009 (2011); C. S. Reynolds, M. A. Nowak, *Phys. Rept.* **377**, 389-466 (2003).
- [31] C. Bambi, *Europhys. Lett.* **94**, 50002 (2011); *JCAP* **1105**, 009 (2011); arXiv:1104.2218 (2011).
- [32] H. Bloemen, K. Bennett, J. J. Blom, W. Collmar, W. Hermsen, G. G. Lichti, D. Morris, V. Schoenfelder *et al.*, *Astron. Astrophys.* **293**, L1 (1995); K. McNaron-Brown, W. N. Johnson, G. V. Jung, R. L. Kinzer, J. D. Kurfess, M. S. Strickman, C. D. Dermer, D. A. Grabelsky *et al.*, *Astrophys. J.* **451**, 575 (1995); V. Schoenfelder, K. Bennett, H. Bloemen, R. Diehl, W. Hermsen, G. Lichti, M. McConnell, J. Ryan *et al.*, *Astron. Astrophys. Suppl.* **120**, 13 (1996).
- [33] J. E. McClintock, R. Shafee, R. Narayan, R. A. Remillard, S. W. Davis, L. -X. Li, *Astrophys. J.* **652**, 518-539 (2006).
- [34] M. A. Abramowicz, *Acta Astronomica* **21**, 221 (1971); F. H. Seguin, *Astrophys. J.* **197**, 745 (1975); J. M. Bardeen, *Astrophys. J.* **162**, 71 (1970).
- [35] M. A. Abramowicz, *Acta Astronomica*, **21**, 81 (1971).
- [36] R. Svensson, *Mon. Not. Roy. Astron. Soc.* **209**, 175-208 (1984).